Hindawi
Journal of Nanomaterials
Volume 2021, Article ID 3806691, 9 pages
https://doi.org/10.1155/2021/3806691

Research Article

Local Surface Plasmonic Resonance, Surface-Enhanced Raman Scattering, Photoluminescence, and Photocatalytic Activity of Hydrothermal Titanate Nanotubes Coated with Ag Nanoparticles

Pham Thi Thuy,[1] Vo Cao Minh,[2] Vo Quang Mai,[1] Nguyen Tri Tuan,[3] Pham Van Tuan,[4] Hoang Ba Cuong,[5] and Nguyen Xuan Sang[6]

[1]*Department of Natural Sciences Education, Saigon University, 273 An Duong Vuong, Ward 3, District 5, Ho Chi Minh City 700000, Vietnam*
[2]*Department of Environmental Sciences, Saigon University, 273 An Duong Vuong, Ward 3, District 5, Ho Chi Minh City 700000, Vietnam*
[3]*Department of Physics, College of Natural Sciences, Campus II, Can Tho University, 3/2 Street, Can Tho City, Vietnam*
[4]*International Training Institute for Materials Science (ITIMS), Hanoi University of Science and Technology, Hanoi 100000, Vietnam*
[5]*The Research Laboratories of Saigon High-Tech-Park, Lot I3, N2 Street, Saigon Hi-Tech-Park, District 9, Ho Chi Minh City 700000, Vietnam*
[6]*Department of Electronics and Telecommunication, Saigon University, 273 An Duong Vuong, Ward 3, District 5, 700000 Ho Chi Minh City, Vietnam*

Correspondence should be addressed to Nguyen Xuan Sang; sangnguyen@sgu.edu.vn

Received 19 May 2021; Revised 16 October 2021; Accepted 28 November 2021; Published 30 December 2021

Academic Editor: Lucien Saviot

In this work, we successfully fabricated homogeneous hydrothermal titanate nanotubes (TNTs) coated with Ag nanoparticles (NPs) and elucidated the role of Ag NPs on local surface plasmonic resonance, surface-enhanced Raman scattering, and the enhanced photocatalytic activity of TNT/Ag nanocomposite. The results showed that the photodegradation process reached equilibrium in just ~5 min for the TNT/Ag nanocomposite, which was much shorter than that of the TNT sample (~90 min). TEM micrographs showed that Ag NPs were well dispersed on the walls of the nanotubes. XRD patterns and Raman spectra indicated that the TNTs were in the monoclinic structure of $H_2Ti_3O_7$. Furthermore, Raman active modes of the TNTs were significantly enhanced in the TNT/Ag sample, which was attributed to surface-enhanced Raman spectroscopy. The enhanced photocatalytic activity of the TNT/Ag sample was explained by UV-vis diffuse reflectance spectroscopy and photoluminescence emission spectroscopy, which showed local surface plasmonic resonance-induced visible light absorption enhancement and effective charge separation, respectively.

1. Introduction

Recently, scientists worldwide have paid much attention to plasmonic photocatalysis [1–3]. The term "plasmonic photocatalysis" could be understood as oxide semiconductors such as ZnO, TiO_2, and WO_3 coated with noble metals that enhance their photocatalytic activity due to the local surface plasmon resonance (LSPR) effect, which can significantly improve visible light absorption. Amongst plasmonic photocatalytic semiconductors, TiO_2 coated with noble metal nanoparticles (NPs) has been widely studied. Many reports on Ag NP coating on TiO_2 showed visible photocatalytic enhancement in both hydrogen production [4–6] and organic dye degradation [7]. Several other works dealt with an anatase TiO_2 nanotube (NT), a highly specific surface area material, which was obtained by annealing the

hydrothermal titanate nanotube at ~400°C or higher [8–12]. These works used XRD characterization to confirm the pure anatase phase of TiO_2 NTs. However, by Raman scattering investigation, our recent work showed that the anatase phase in the annealed titanate NTs was from TiO_2 NPs that were formed by thermal-induced interruption due to the low-thermal stability of titanate NTs, and the titanate NT itself remained in the monoclinic phase [13]. It is worth noting that calcination treatment gives rise to enhanced photocatalytic activity due to the heterojunction formation of TNTs and TiO_2 NPs.

In this work, we fabricated titanate NTs (TNTs) and Ag NPs coating TNT (TNT/Ag) samples and studied the photodegradation of methylene blue dye under visible light exposure. Surface morphology and crystal structure of synthesized samples were characterized by transmission electron microscopy (TEM), energy-dispersive X-ray spectroscopy (EDX), X-ray diffractometry (XRD), and Raman spectroscopy. In order to obtain insights into the enhanced photocatalytic activity, optical properties of synthesized samples were investigated by UV-vis diffuse reflectance spectroscopy (DRS) and photoluminescence (PL) emission spectroscopy, in which bandgap and charge separation of synthesized samples were identified.

2. Material and Methods

2.1. Chemicals. All chemicals were purchased and used without further purification. The chemicals were TiO_2 powder (anatase phase, Merck), $AgNO_3$ 0.1 N (Merck, purity 99.99%), $NaBH_4$ (Merck, 99.99%), NaOH (Merck, 99.9%), HCl (Xilong, 37%), ethanol (Sigma Aldrich, 99.9%), and bidistilled water.

2.2. Synthesis of TNT. The hydrothermal synthesis of TNT in sodium hydroxyl solution was reported previously [14, 15]. Typically, 0.84 g TiO_2 was magnetically stirred in an 80 ml 10 M NaOH solution for 30 min. Then, the resulting solution was transferred to teflon autoclave for hydrothermal processing at 150°C for 24 h. After the hydrothermal process, the autoclave was naturally cooled down to room temperature. The resulting wet powder was collected and immersed in a 0.1 M HCl solution for 30 min and then washed with bidistilled water until the pH reached 7. Finally, the powder was put in an oven at 100°C for hours until completely dry.

2.3. Synthesis of TNT/Ag Nanocomposite. In order to attach Ag NPs onto the TNTs, a reduction process to form Ag from Ag^+ was carried out, as described previously [16]. Typically, firstly, 0.5 g TNTs were dispersed into 30 ml bidistilled water. Secondly, the resultant solution was, drop by drop, added to 0.1 M $AgNO_3$ with continuous magnetic stirring until a ratio of Ag to Ti of 0.05 was reached. Thirdly, the powder was collected by centrifugation with a velocity of 5000 rounds per second, and then, $NaBH_4$ was added as the reduction agent. Finally, the powder was washed, filtered, and dried at 90°C, and the final product was denoted as TNT/Ag.

3. Results and Discussion

3.1. Surface Morphological and Structural Properties. Figure 1 shows transmission electron micrographs of TNT and TNT/Ag samples. Figures 1(a) and 1(b) indicate that the nanotubes were formed by the hydrothermal method with a homogeneous diameter of ~8 nm, and the length varied from 20 nm to 50 nm. Figures 1(c) and 1(d) clearly show TNT/Ag composites in which uniform Ag nanoparticles with a size of ~3 nm were attached and well distributed on the TNT surface. EDX mapping analysis of TNT/Ag, as shown in Figure 1(e), indicates the homogeneous distribution of Ag NPs on the TNT surface.

Figure 2(a) shows XRD patterns of synthesized samples. In general, XRD patterns of TNT and TNT/Ag were similar to the monoclinic phase of $H_2Ti_3O_7$, with diffraction angles (2θ) of 9.40°, 24.18°, 28.26°, and 48.22° corresponding to directions of (001), (110), (211), and (020) [14, 17, 18]. The structural transformation from anatase TiO_2 to monoclinic titanate with a layer structure was reported previously [19–21]. Chen et al. showed that the spacing distance of the interlayer was about 0.78 nm, which was formed by conjugated edge-sharing TiO_6 octahedrons [22]. Hydrogen atoms in the $H_2Ti_3O_7$ nanotube were located between interlayers, which replaced Na atoms in the as-prepared sodium titanate nanotube through the HCl postwashing treatment [23]. Because of the weak bonding of the H atom in the nanotube, the monoclinic crystal of $H_2Ti_3O_7$ could easily be transformed back to anatase TiO_2 by simple annealing [13]. It is worth noting that after attachment of the Ag nanoparticle, the diffraction intensity of (211) direction was recognisably increased.

Figure 2(b) shows Raman active modes of TNT and TNT-Ag appearing at 192, 275.5, 445.6, and 668.3 cm^{-1}. These active modes represent Raman characteristic vibrations of the titanate tubular structure [24–26], which were sharply enhanced in the TNT/Ag due to the surface-enhanced Raman scattering (SERS) effect by loading Ag nanoparticles onto the TNTs. It can be seen that there was no anatase active Raman mode in the synthesized samples. Hence, the hydrothermal process fully transformed the anatase TiO_2 to the monoclinic titanate nanotube. The enhanced Raman scattering in TNT/Ag proposed a useful method to characterize the Raman vibration modes of low-crystalline structures of TNT, whose Raman modes were sometimes reportedly hard to distinguish [27] because of the low crystal structure [26, 28].

The chemical composition, oxidization state, and the presence of Ag nanoparticles in TNT/Ag nanocomposite were determined by utilizing XPS analysis as seen in Figure 3. Particularly, Figure 3(a) shows that the TNT/Ag sample possessed three major elements, namely, Ti, O, and Ag, corresponding Ti 2p, O 1s, and Ag 3d spectra, accordingly. Regarding XPS spectra of the Ag 3d region (Figure 3(b)), two emerging peaks were located at 367.4 eV and 373.4 eV, which are assigned to characteristic binding energy of Ag $3d_{5/2}$ and Ag $3d_{3/2}$ spin states [29]. As proposed in previous studies [8, 30, 31], these peaks with a distance around 6 eV originated from Ag nanoparticles

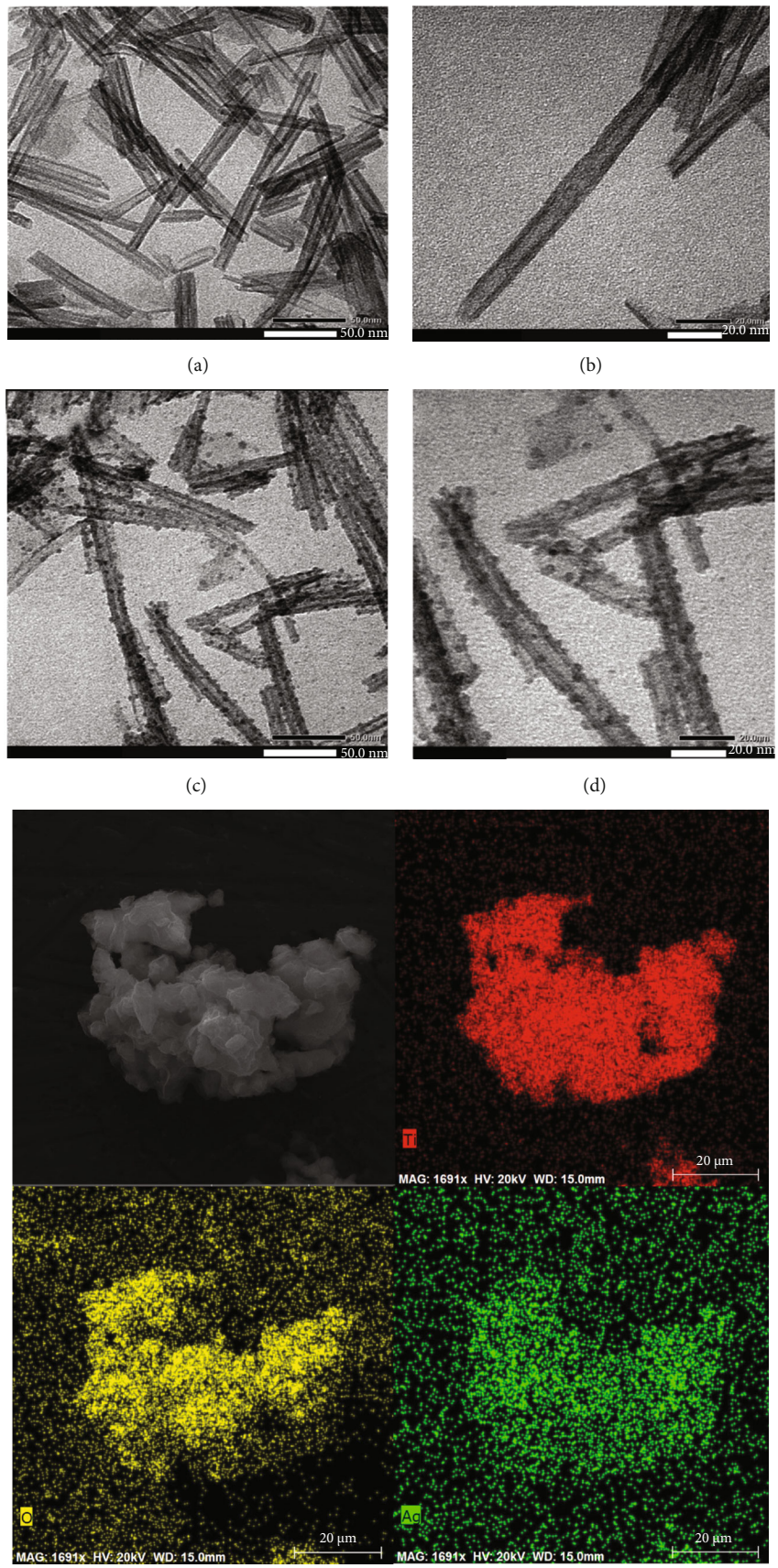

Figure 1: TEM micrographs of TNT (a, b), TNT/Ag (c, d), and EDX elemental maps of Ti, O, and Ag in TNT/Ag.

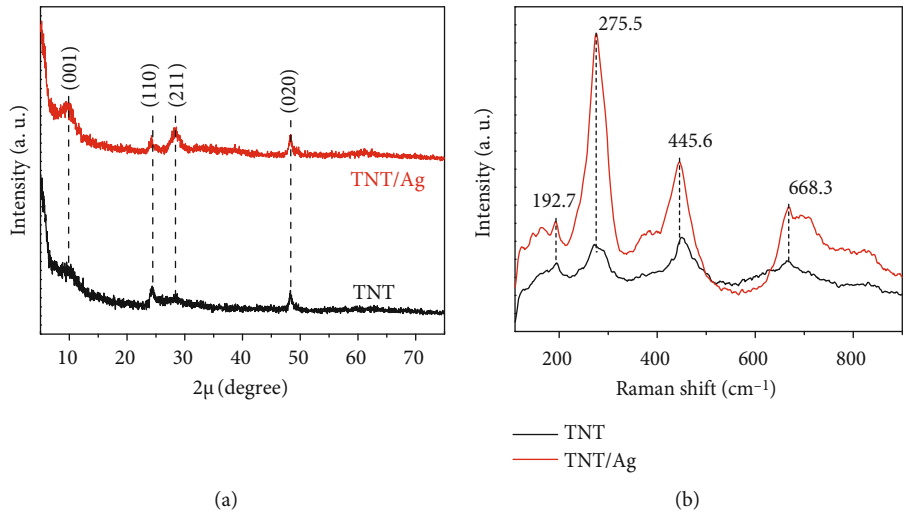

Figure 2: (a) XRD patterns and (b) Raman spectra of TNT and TNT/Ag samples.

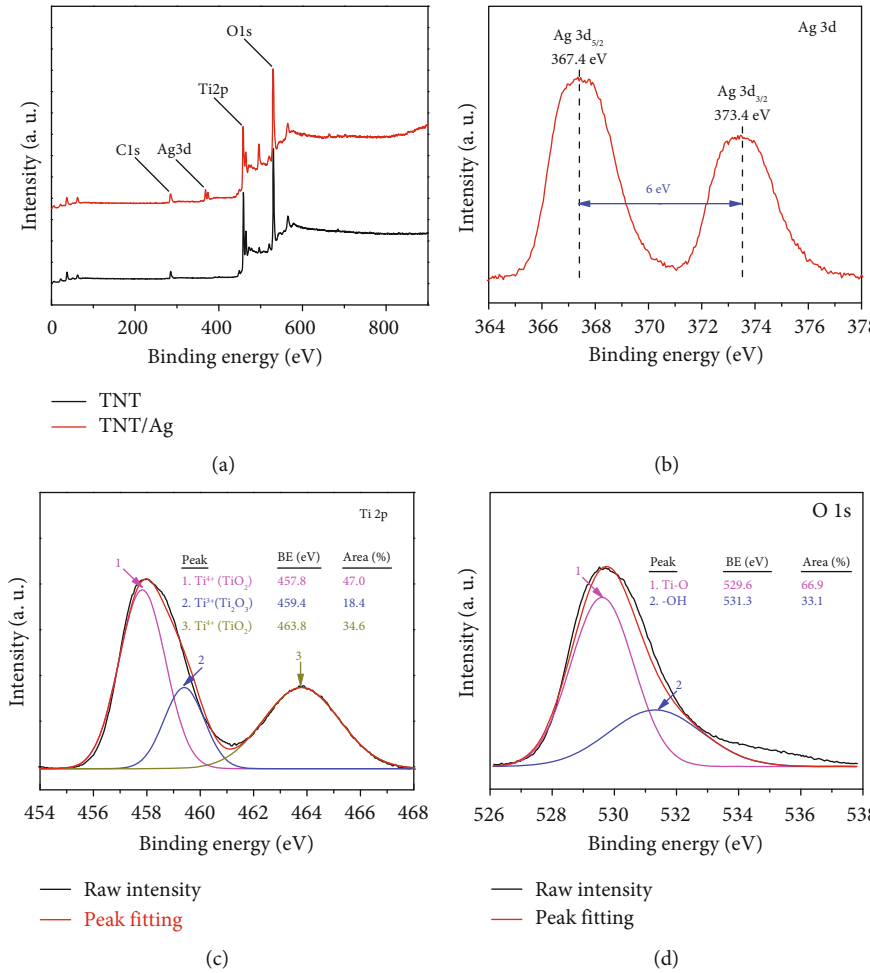

Figure 3: (a) XPS survey spectrum; XPS spectra of TNT/Ag: (b) Ag 3d, (c) Ti 2p, and (d) O 1s.

anchoring onto TNT's surface since Ag^{+} ($AgNO_3$) was reduced to Ag^{o} state in the fabrication process. By using Gaussian peak fitting, Ti 2p XPS of TNT/Ag could be divided into three distinct peaks at 457.8 eV ($Ti^{4+2}p_{3/2}$), 459.4 eV ($Ti^{3+2}p_{1/2}$), and 463.8 eV ($Ti^{4+2}p_{1/2}$) as depicted in Figure 3(c). Whereas two main peaks at 457.8 and 463.8 eV with 81.6% (peak area) belonged to Ti^{4+} state in TiO_2 structure, there is an individual peak at 459.4 eV with only 18.4%

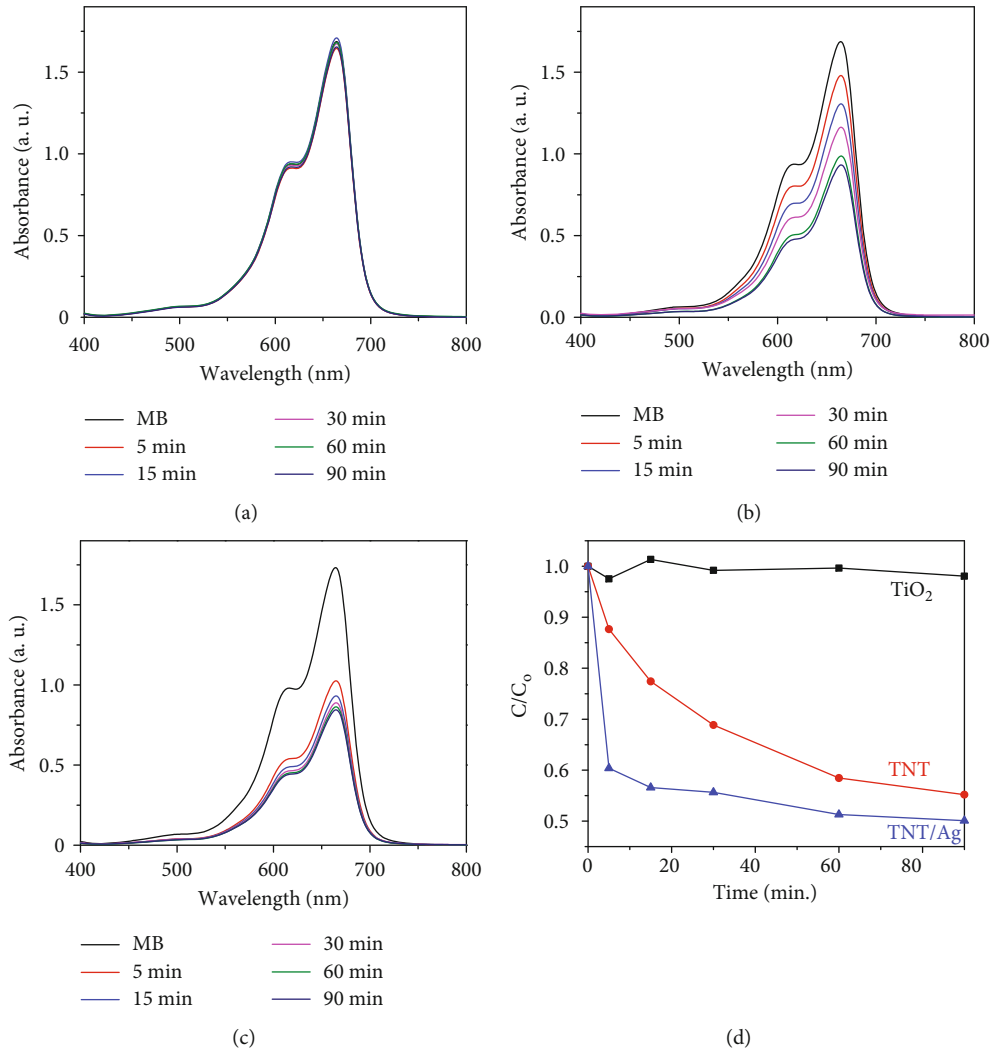

Figure 4: Sequence of MB degradation under visible light exposure of (a) starting TiO_2, (b) TNT, and (c) TNT/Ag. (d) The photodegradation collected at the characteristic MB absorption peak at 644 nm.

(peak area) ascribed to Ti^{3+} state which is related to Ti_2O_3 structure [4, 32]. Additionally, O 1s spectra had two deconvoluted peaks, one from 529.6 eV and the other from 531.3 eV attributing to Ti-O bond and surface adsorbed OH groups [33], respectively, which are shown in Figure 3(d). Importantly, there was a negative shift of around 0.6 eV and 0.4 eV in terms of Ti 2p and O 1s spectra of TNT/Ag, respectively, compared to that of pure TNT (as seen in Figure S1). This is due to the connection of Ti-O bond in the TNT structure and Ag nanoparticles on its surface through electrostatic or covalent interaction to form Ti-O-Ag networks [34].

3.2. Photocatalytic Test. We added 0.01 g catalyst (starting TiO_2, TNT, or TNT/Ag) in a 250 ml solution of 25 ppm methylene blue (MB) for photocatalytic evaluation of MB degradation. After that, the powders were simultaneously stirred in the dark for 60 min until the adsorption reached an equilibrium state. Then, the visible photocatalytic measurement was carried out by irradiating the resulting solution under natural solar light on a sunny day. We started measuring MB degradation at different times of 5, 15, 30, 60, and 90 min under sunlight irradiation. Figure 4 shows the sequence of MB absorption spectra over exposure times (Figures 4(a)–4(c)) and the degradation efficiency of MB by using its characteristic absorption peak at 664 nm (Figure 4(d)), where C and C_0 were concentrations of MB at the time of measuring and at the beginning of the experiment, respectively. It showed that the time for MB degradation to reach equilibrium was short (~5 min) in comparison to that of the TNT sample (~90 min), with MB degradation of 40% and 12%, respectively. However, after 90 min of exposure, the photodegradation efficiency of TNT and TNT/Ag, which was ~45% and ~50%, respectively, was not much different. Hence, photocatalytic activity of TNT/Ag was significantly enhanced in terms of time compared to the TNT sample. In order to understand the mechanism of the enhancement, in the next section, we will investigate the optical properties of the synthesized samples by DRS and PL measurements.

3.3. Optical Properties. Figure 5 shows UV-vis DRS spectra of the synthesized samples and the bandgaps determined

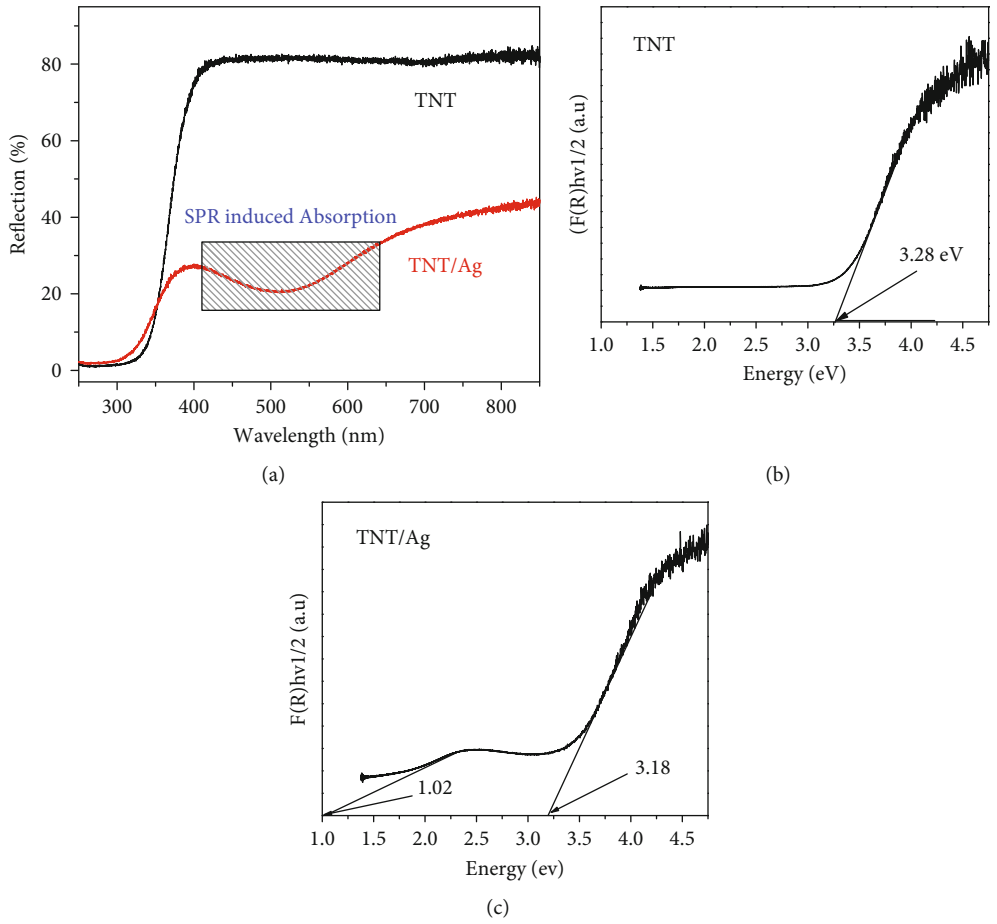

Figure 5: (a) UV-vis diffuse reflectance spectra of TNT and TNT/Ag; bandgaps were determined by the Kubelka-Munk function of (b) TNT and (c) TNT/Ag.

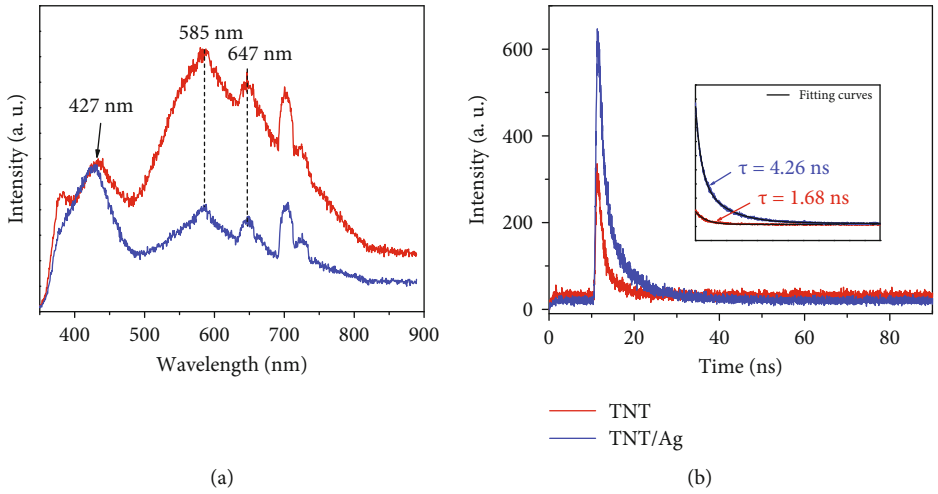

Figure 6: Normalized photoluminescence emission and time-resolved photoluminescence spectra of TNT and TNT/Ag.

by Tauc's plot using the Kubelka-Munk function [35]. In general, the DRS spectra in Figure 4(a) showed improvements in visible light absorption of the TNT/Ag composite, which played an important role in the enhanced photocatalytic activity. Furthermore, local surface plasmon resonance- (LSPR-) enhanced absorption was revealed in the range of 400–600 nm, which was around the characteristic strong absorption range of Ag nanoparticles [36, 37]. Hu and coworkers reported that the broad absorption peak was possibly due to the nonuniformity of Ag nanoparticles [38]. However, as shown in TEM images, Ag NPs in TNT/Ag were highly uniform with a size of 3 nm, and the low

concentration of Ag NPs could be attributed to the broadening of the resonant peak. The bandgap values of the synthesized samples were estimated from the DRS spectra using the Kubelka-Munk method [14, 35] shown in Figures 5(b) and 5(c), where the values were ~3.28 eV and ~3.18 eV for TNT and TNT/Ag, respectively. The bandgap decrease in the composite sample was attributed to the increase of the Fermi level when n-type TNT semiconductor contacted with metallic Ag nanoparticles [39]. The small "bump" signal at lower energy in Figure 4(c) was induced by the SPR effect which was observed in the reflectance spectra. Hence, by the DRS measurement, TNT/Ag showed that Ag NPs induced an LSPR effect in which the visible light absorption capacity of the sample significantly increased, which could be assigned to the enhanced photocatalytic activity.

Both enhanced light harvesting and bandgap reduction in the composite sample were beneficial to photocatalytic improvement [40–43]. Another important factor for enhanced photocatalytic activity was the radiative combination rate that brought about information of the photoinduced carriers' lifetimes, which were usually characterized by the photoluminescence (PL) emission intensity. Figure 6(a) shows normalized PL emission intensities of synthesized samples, which indicated that the radiative recombination rate of photoinduced electron-hole pairs was possibly reduced in the TNT/Ag composite [40, 44, 45]. Typically, PL signals that appeared at 427 nm (2.90 eV), 585 nm (2.12 eV), and 647 nm (1.92 eV) were assigned to radiative recombinations of band-band excitons, conduction band electron-singly ionized oxygen vacancy (V_O^+), and electron trap-valence band hole, respectively [44, 46]. The lower the radiative recombination, the longer the carrier lifetime and, thus, the higher the possibility of photoinduced carriers interacting to degrade organic compounds [47]. However, an unwanted case known as nonradiative emission could happen to reduce the PL emission intensity when the coated materials cover the host surface [48]. This phenomenon was called the PL quenching effect, which many previous photocatalytic studies did not pay much attention to whether the decrease of PL emission intensity was because of the charge separation or the PL quenching effect. In order to clarify the decreasing recombination rate in the composite, a time-resolved PL measurement was carried out, as shown in Figure 6(b). The excitation wavelength of 466 nm from a 0.5 μW laser source with 5 ps pulses was used. The fitting decay curves of time-resolved PL spectra shown in the subfigure of Figure 6(b) indicated that the photoelectron lifetime of TNT/Ag of ~4.26 ns was significantly longer than that of TNT, which was ~1.68 ns. Hence, the recombination rate of the composite sample was about 2.75-fold longer than that of TNT; thus, photoexcited carriers would have more time in the solution vicinity to promote highly oxidative and reductive radicals to decompose the organic dye [49, 50].

4. Conclusions

In this work, we successfully fabricated hydrothermal TNTs coated with Ag NPs by a facile two-step method. The photocatalytic activity of the TNT/Ag composite was investigated by measuring the degradation of MB. The MB degradation equilibrium state was reached only after 5 min of sunlight irradiation with a degradation efficiency of ~40%. The mechanism of enhanced photocatalytic activity was revealed by DRS and PL studies, which, respectively, showed LSPR-induced visible light absorption and charge separation improvement, i.e., photoinduced carrier lifetimes of ~1.68 ns for TNTs and ~4.26 ns for TNT/Ag. Furthermore, the SERS effect presented in the TNT/Ag sample was useful to characterize the TNT layered monoclinic microstructure.

Data Availability

Data is available on request.

Conflicts of Interest

The authors declare that they have no conflicts of interest.

Acknowledgments

This research is funded by the Vietnam National Foundation for Science and Technology Development (NAFOSTED) under grant number 103.02-2019.362. NXS acknowledges the CERIC-ERIC Consortium for access to the XPS and FE-SEM experimental facilities at the Charles University of Prague, Czech Republic, and travel and accommodation support. PTT and NXS acknowledge Saigon University key project number TĐ2020-45.

Supplementary Materials

Figure S1: XPS spectra of TNT and TNT/Ag: (a) Ti 2p and (b) O 1s. *(Supplementary Materials)*

References

[1] W. Hou and S. B. Cronin, "A review of surface plasmon resonance-enhanced photocatalysis," *Advanced Functional Materials*, vol. 23, no. 13, pp. 1612–1619, 2013.

[2] X. Zhang, Y. L. Chen, R. S. Liu, and D. P. Tsai, "Plasmonic photocatalysis," *Reports on Progress in Physics*, vol. 76, no. 4, article 046401, 2013.

[3] R. Wang, J. Shen, K. Sun, H. Tang, and Q. Liu, "Enhancement in photocatalytic activity of CO_2 reduction to CH_4 by 0D/2D Au/TiO_2 plasmon heterojunction," *Applied Surface Science*, vol. 493, pp. 1142–1149, 2019.

[4] D. Gogoi, A. Namdeo, A. K. Golder, and N. R. Peela, "Ag-doped TiO_2 photocatalysts with effective charge transfer for highly efficient hydrogen production through water splitting," *International Journal of Hydrogen Energy*, vol. 45, no. 4, pp. 2729–2744, 2020.

[5] N. Naseri, H. Kim, W. Choi, and A. Z. Moshfegh, "Optimal Ag concentration for H_2 production via Ag:TiO_2 nanocomposite thin film photoanode," *International Journal of Hydrogen Energy*, vol. 37, no. 4, pp. 3056–3065, 2012.

[6] A. Sreedhar, T. V. M. Sreekanth, J. H. Kwon, J. Yi, Y. Sohn, and J. S. Gwag, "Ag nanoparticles decorated ion-beam-assisted TiO_2 thin films for tuning the water splitting activity from UV to visible light harvesting," *Ceramics International*, vol. 43, no. 15, pp. 12814–12821, 2017.

[7] N. R. Khalid, U. Mazia, M. B. Tahir, N. A. Niaz, and M. A. Javid, "Photocatalytic degradation of RhB from an aqueous solution using Ag_3PO_4/N-TiO_2 heterostructure," *Journal of Molecular Liquids*, vol. 313, article 113522, 2020.

[8] D. Yang, Y. Sun, Z. Tong, Y. Tian, Y. Li, and Z. Jiang, "Synthesis of Ag/TiO2nanotube heterojunction with improved visible-light photocatalytic performance inspired by bioadhesion," *The Journal of Physical Chemistry C*, vol. 119, no. 11, pp. 5827–5835, 2015.

[9] C. Y. Tsai, C. W. Liu, H. C. Hsi, K. S. Lin, Y. W. Lin, and L. C. Lai, "Synthesis of Ag-modified TiO_2nanotube and its application in photocatalytic degradation of dyes and elemental mercury," *Journal of Chemical Technology & Biotechnology*, vol. 94, no. 10, pp. 3251–3262, 2019.

[10] N. Pugazhenthiran, S. Murugesan, and S. Anandan, "High surface area Ag-TiO_2 nanotubes for solar/visible- light photocatalytic degradation of ceftiofur sodium," *Journal of Hazardous Materials*, vol. 263, Part 2, pp. 541–549, 2013.

[11] M. S.-L. Yee, P. S. Khiew, S. S. Lim et al., "Enhanced marine antifouling performance of silver-titania nanotube composites from hydrothermal processing," *Colloids and Surfaces A: Physicochemical and Engineering Aspects*, vol. 520, pp. 701–711, 2017.

[12] M. Mangayayam, J. Kiwi, S. Giannakis et al., "FeOx magnetization enhancing _E. coli_ inactivation by orders of magnitude on Ag-TiO_2 nanotubes under sunlight," *Applied Catalysis B: Environmental*, vol. 202, pp. 438–445, 2017.

[13] N. X. Sang and V. C. Minh, "Thermal annealing-induced self-junction of hydrothermal titanate nanotubes/TiO_2nanoparticles with enhanced photocatalytic activity," *Nanotechnology*, vol. 31, no. 43, article 435703, 2020.

[14] T. D. Phan, C. M. Vo, T. M. T. Tran, T. L. A. Luu, and X. S. Nguyen, "Structural and bandgap properties of titanium dioxide nanotube/graphene oxide composites prepared by a facile hydrothermal method," *Materials Research Express*, vol. 6, no. 10, article 105054, 2019.

[15] P. Van Viet, T. H. Huy, N. X. Sang, C. M. Thi, and L. Van Hieu, "One-step hydrothermal synthesis and characterisation of SnO_2 nanoparticle-loaded TiO_2 nanotubes with high photocatalytic performance under sunlight," *Journal of Materials Science*, vol. 53, no. 5, pp. 3364–3374, 2018.

[16] Y. Wen, H. Ding, and Y. Shan, "Preparation and visible light photocatalytic activity of Ag/TiO_2/graphene nanocomposite," *Nanoscale*, vol. 3, no. 10, pp. 4411–4417, 2011.

[17] L. B. Arruda, C. M. Santos, M. O. Orlandi, W. H. Schreiner, and P. N. Lisboa-Filho, "Formation and evolution of TiO_2 nanotubes in alkaline synthesis," *Ceramics International*, vol. 41, no. 2, pp. 2884–2891, 2015.

[18] A. Eguia-Barrio, E. Castillo-Martinez, M. Zarrabeitia, M. A. Munoz-Marquez, M. Casas-Cabanas, and T. Rojo, "Structure of $H_2Ti_3O_7$ and its evolution during sodium insertion as anode for Na ion batteries," *Physical Chemistry Chemical Physics*, vol. 17, no. 10, pp. 6988–6994, 2015.

[19] H. Ou and S. Lo, "Review of titania nanotubes synthesized via the hydrothermal treatment: fabrication, modification, and application," *Separation and Purification Technology*, vol. 58, no. 1, pp. 179–191, 2007.

[20] S. Muniyappan, T. Solaiyammal, K. Sudhakar, A. Karthigeyan, and P. Murugakoothan, "Conventional hydrothermal synthesis of titanate nanotubes: systematic discussions on structural, optical, thermal and morphological properties," *Modern Electronic Materials*, vol. 3, no. 4, pp. 174–178, 2017.

[21] D. V. Bavykin, V. N. Parmon, A. A. Lapkin, and F. C. Walsh, "The effect of hydrothermal conditions on the mesoporous structure of TiO_2 nanotubes," *Journal of Materials Chemistry*, vol. 14, no. 22, pp. 3370–3377, 2004.

[22] Q. Chen, G. H. Du, S. Zhang, and L. M. Peng, "The structure of trititanate nanotubes," *Acta Crystallographica Section B Structural Science*, vol. 58, no. 4, pp. 587–593, 2002.

[23] S. Zhang, Q. Chen, and L. M. Peng, "Structure and formation ofH2Ti3O7nanotubes in an alkali environment," *Physical Review B*, vol. 71, no. 1, 2005.

[24] B. Sharma, R. R. Frontiera, A.-I. Henry, E. Ringe, and R. P. Van Duyne, "SERS: materials, applications, and the future," *Materials Today*, vol. 15, no. 1-2, pp. 16–25, 2012.

[25] T. Gao, H. Fjellvag, and P. Norby, "Crystal structures of titanate nanotubes: a Raman scattering study," *Inorganic Chemistry*, vol. 48, no. 4, pp. 1423–1432, 2009.

[26] M. A. Cortés-Jácome, G. Ferrat-Torres, L. F. F. Ortiz et al., "In situ thermo-Raman study of titanium oxide nanotubes," *Catalysis Today*, vol. 126, no. 1-2, pp. 248–255, 2007.

[27] Á. Kukovecz, K. Kordás, J. Kiss, and Z. Kónya, "Atomic scale characterization and surface chemistry of metal modified titanate nanotubes and nanowires," *Surface Science Reports*, vol. 71, no. 3, pp. 473–546, 2016.

[28] G. Potari, D. Madarasz, L. Nagy et al., "Rh-induced support transformation phenomena in titanate nanowire and nanotube catalysts," *Langmuir*, vol. 29, no. 9, pp. 3061–3072, 2013.

[29] X. Chong, B. Zhao, R. Li, W. Ruan, and X. Yang, "Photocatalytic degradation of rhodamine 6G on Ag modified TiO_2 nanotubes: surface-enhanced Raman scattering study on catalytic kinetics and substrate recyclability," *Colloids and Surfaces A: Physicochemical and Engineering Aspects*, vol. 481, pp. 7–12, 2015.

[30] M.-Z. Ge, C.-Y. Cao, S.-H. Li et al., "In situ plasmonic Ag nanoparticle anchored TiO2nanotube arrays as visible-light-driven photocatalysts for enhanced water splitting," *Nanoscale*, vol. 8, no. 9, pp. 5226–5234, 2016.

[31] A. Perumal, S. Kannan, and R. Nallaiyan, "Silver nanoparticles incorporated polyaniline on TiO_2 nanotube arrays: a nanocomposite platform to enhance the biocompatibility and antibiofilm," *Surfaces and Interfaces*, vol. 22, article 100892, 2021.

[32] X. Jiang, Y. Zhang, J. Jiang et al., "Characterization of oxygen vacancy associates within hydrogenated TiO_2: a positron annihilation study," *The Journal of Physical Chemistry C*, vol. 116, no. 42, pp. 22619–22624, 2012.

[33] B. Bharti, S. Kumar, H.-N. Lee, and R. Kumar, "Formation of oxygen vacancies and Ti^{3+} state in TiO_2 thin film and enhanced optical properties by air plasma treatment," *Scientific Reports*, vol. 6, no. 1, pp. 1–12, 2016.

[34] S. P. Deshmukh, S. B. Mullani, V. B. Koli et al., "Ag nanoparticles connected to the surface of TiO_2electrostatically for antibacterial photoinactivation studies," *Photochemistry and Photobiology*, vol. 94, no. 6, pp. 1249–1262, 2018.

[35] R. López and R. Gómez, "Band-gap energy estimation from diffuse reflectance measurements on sol–gel and commercial TiO_2: a comparative study," *Journal of Sol-Gel Science and Technology*, vol. 61, no. 1, pp. 1–7, 2012.

[36] S. A. Ansari, M. M. Khan, M. O. Ansari, and M. H. Cho, "Silver nanoparticles and defect-induced visible light photocatalytic and photoelectrochemical performance of $_2$ nanocomposite," *Solar Energy Materials and Solar Cells*, vol. 141, pp. 162–170, 2015.

[37] A. Ziashahabi, M. Prato, Z. Dang, R. Poursalehi, and N. Naseri, "The effect of silver oxidation on the photocatalytic activity of Ag/ZnO hybrid plasmonic/metal-oxide nanostructures under visible light and in the dark," *Scientific Reports*, vol. 9, no. 1, article 11839, 2019.

[38] C. Hu, Y. Lan, J. Qu, X. Hu, and A. Wang, "Ag/AgBr/TiO_2 visible light photocatalyst for destruction of azodyes and bacteria," *The Journal of Physical Chemistry. B*, vol. 110, no. 9, pp. 4066–4072, 2006.

[39] W. Liu, J. Shen, H. Chen et al., "Localized surface plasmon resonance induced band gap regulation governing the excellent photocatalytic performance of Ag/g-C_3N_4heterostructure," *Journal of Nanoscience and Nanotechnology*, vol. 19, no. 9, pp. 5582–5590, 2019.

[40] K. Thiyagarajan, S. Samuel, and S. G. Babu, "NiO/C_3N_4: hybrid photocatalyst for the enhanced photodegradation of organic pollutant under visible light," *Materials Research Express*, vol. 5, no. 11, article 115503, 2018.

[41] C.-Y. Tsai, C.-W. Liu, C. Fan, H.-C. Hsi, and T.-Y. Chang, "Synthesis of a SnO_2/TNT heterojunction nanocomposite as a high-performance photocatalyst," *The Journal of Physical Chemistry C*, vol. 121, no. 11, pp. 6050–6059, 2017.

[42] T. J. Wong, F. J. Lim, M. Gao, G. H. Lee, and G. W. Ho, "Photocatalytic H_2 production of composite one-dimensional TiO_2 nanostructures of different morphological structures and crystal phases with graphene," *Catalysis Science & Technology*, vol. 3, no. 4, p. 1086, 2013.

[43] Y. Wu, Z. Liu, Y. Li, J. Chen, X. Zhu, and P. Na, "WS_2 nanodots-modified TiO_2 nanotubes to enhance visible-light photocatalytic activity," *Materials Letters*, vol. 240, pp. 47–50, 2019.

[44] C. C. Mercado, F. J. Knorr, J. L. McHale, S. M. Usmani, A. S. Ichimura, and L. V. Saraf, "Location of hole and electron traps on nanocrystalline anatase TiO_2," *The Journal of Physical Chemistry C*, vol. 116, no. 19, pp. 10796–10804, 2012.

[45] Y. Min, K. Zhang, W. Zhao, F. Zheng, Y. Chen, and Y. Zhang, "Enhanced chemical interaction between TiO_2 and graphene oxide for photocatalytic decolorization of methylene blue," *Chemical Engineering Journal*, vol. 193-194, pp. 203–210, 2012.

[46] D. K. Pallotti, L. Passoni, P. Maddalena, F. Di Fonzo, and S. Lettieri, "Photoluminescence mechanisms in anatase and rutile TiO_2," *The Journal of Physical Chemistry C*, vol. 121, no. 16, pp. 9011–9021, 2017.

[47] R. Wang, J. Shen, W. Zhang et al., "Build-in electric field induced step-scheme TiO_2/$W_{18}O_{49}$ heterojunction for enhanced photocatalytic activity under visible-light irradiation," *Ceramics International*, vol. 46, no. 1, pp. 23–30, 2020.

[48] S. X. Nguyen, T. Thanh Tung, P. T. Lan Huong, N. H. Tho, and D. Losic, "Heterojunction of graphene and titanium dioxide nanotube composites for enhancing photocatalytic activity," *Journal of Physics D: Applied Physics*, vol. 51, no. 26, article 265304, 2018.

[49] X.-S. Nguyen, M.-Q. Nguyen, X.-T. Trinh, A. C. Joita, and S. V. Nistor, "Correlation of native point defects and photocatalytic activity of annealed ZnO nanoparticle studied by electron spin resonance and photoluminescence emission," *Semiconductor Science and Technology*, vol. 35, no. 9, article 095035, 2020.

[50] Q. Zhang, N. Bao, X. Wang et al., "Advanced fabrication of chemically bonded graphene/TiO_2 continuous fibers with enhanced broadband photocatalytic properties and involved mechanisms exploration," *Scientific Reports*, vol. 6, no. 1, article 38066, 2016.